A&A 545, A32 (2012)
DOI: 10.1051/0004-6361/201219401

Astronomy & Astrophysics

Chemical abundances of 1111 FGK stars from the HARPS GTO planet search program

Galactic stellar populations and planets⋆,⋆⋆,⋆⋆⋆

V. Zh. Adibekyan[1], S. G. Sousa[1,2], N. C. Santos[1,3], E. Delgado Mena[1], J. I. González Hernández[2,4], G. Israelian[2,4], M. Mayor[5], and G. Khachatryan[1,3]

[1] Centro de Astrofísica da Universidade do Porto, Rua das Estrelas, 4150-762 Porto, Portugal
e-mail: Vardan.Adibekyan@astro.up.pt
[2] Instituto de Astrofísica de Canarias, 38200 La Laguna, Tenerife, Spain
[3] Departamento de Física e Astronomia, Faculdade de Ciências da Universidade do Porto, Portugal
[4] Departamento de Astrofísica, Universidad de La Laguna, 38206 La Laguna, Tenerife, Spain
[5] Observatoire de Genève, Université de Genève, 51 Ch. des Mailletes, 1290 Sauverny, Switzerland

Received 12 April 2012 / Accepted 10 July 2012

ABSTRACT

Context. We performed a uniform and detailed abundance analysis of 12 refractory elements (Na, Mg, Al, Si, Ca, Ti, Cr, Ni, Co, Sc, Mn, and V) for a sample of 1111 FGK dwarf stars from the HARPS GTO planet search program. Of these stars, 109 are known to harbor giant planetary companions and 26 stars are exclusively hosting Neptunians and super-Earths.
Aims. The two main goals of this paper are to investigate whether there are any differences between the elemental abundance trends for stars of different stellar populations and to characterize the planet host and non-host samples in terms of their [X/H]. The extensive study of this sample, focused on the abundance differences between stars with and without planets will be presented in a parallel paper.
Methods. The equivalent widths of spectral lines were automatically measured from HARPS spectra with the ARES code. The abundances of the chemical elements were determined using an LTE abundance analysis relative to the Sun, with the 2010 revised version of the spectral synthesis code MOOG and a grid of Kurucz ATLAS9 atmospheres. To separate the Galactic stellar populations we applied both a purely kinematical approach and a chemical method.
Results. We found that the chemically separated (based on the Mg, Si, and Ti abundances) thin- and thick disks are also chemically disjunct for Al, Sc, Co, and Ca. Some bifurcation might also exist for Na, V, Ni, and Mn, but there is no clear boundary of their [X/Fe] ratios. We confirm that an overabundance in giant-planet host stars is clear for all studied elements.We also confirm that stars hosting only Neptunian-like planets may be easier to detect around stars with similar metallicities than around non-planet hosts, although for some elements (particulary α-elements) the lower limit of [X/H] is very abrupt.

Key words. stars: abundances – planetary systems – stars: fundamental parameters – Galaxy: disk – solar neighborhood – stars: kinematics and dynamics

1. Introduction

High-precision radial velocity measurements resulted in the detection of the first extra-solar planetary system surrounding a main-sequence star similar to our own in 1995 (Mayor & Queloz 1995). Observational progress in extra-solar planet detection and characterization is now moving rapidly on several fronts. More than 750 planetary companions have already been found orbiting late-type stars[1]. The total number of planet-harboring systems that are found using Doppler technique is approaching 500. A strong input for this number was made by several dedicated planet-search programs that systematically monitor the sky. Among these programs, the HARPS planet search program made a special contribution. The high spectral resolution and most importantly the long-term stability of the HARPS spectrograph (Mayor et al. 2003) allowed discovering a fairly large number of new planets, including the large majority of the known planets with masses near the mass of Neptune or below (e.g. Santos et al. 2004b; Lovis et al. 2006; Mayor et al. 2009, 2011).

Shortly after the discovery of the first extra-solar planet, Gonzalez (1998), based on a small sample of eight planet-host stars (PHS), suggested that PHSs tend to be metal-rich compared with the nearby field FGK stars that are known to host no-planet. The metal-rich nature of the PHSs have been confirmed in subsequent papers (e.g. Gonzalez et al. 2001; Santos et al. 2001, 2003, 2004a, 2005; Laws et al. 2003; Fischer & Valenti 2005; Gilli et al. 2006; Udry et al. 2006; Ecuvillon et al. 2007; Sousa et al. 2008; Neves et al. 2009; Johnson et al. 2010; Kang et al. 2011). This tendency for giant planets that orbit

⋆ Based on observations collected at the La Silla Paranal Observatory, ESO (Chile) with the HARPS spectrograph at the 3.6-m telescope (ESO runs ID 72.C-0488, 082.C-0212, and 085.C-0063).
⋆⋆ Full Tables 4, 5, and the table with EWs of the lines are only available at the CDS via anonymous ftp to cdsarc.u-strasbg.fr (130.79.128.5) or via http://cdsarc.u-strasbg.fr/viz-bin/qcat?J/A+A/545/A32
⋆⋆⋆ Figure A.1 is available in electronic form at http://www.aanda.org
[1] http://exoplanet.eu/

metal-rich stars strongly supports the core-accretion model of planet formation (e.g. Pollack et al. 1996). This implies that core accretion (Ida & Lin 2004; Mordasini et al. 2009) and not disk-instability (Boss 1997) is the main working mechanism for the formation of giant planets. Interestingly, recent studies show that Neptune and super-Earth-class planets may easier form in a low-metal-content environment (e.g. Udry et al. 2006; Sousa et al. 2008, 2011a; Ghezzi et al. 2010; Mayor et al. 2011; Buchhave et al. 2012).

Most spectroscopic studies are in general limited to small samples of a few hundred comparison stars and less than one hundred PHSs at most, and only a few studies have been based on samples as large as 1000 stars (e.g. Gazzano et al. 2010; Gazzano 2011; Petigura & Marcy 2011). In order to minimize the errors, one needs to have large and homogeneous samples with reliable measurements of their chemical features.

In this paper, we present a uniform spectroscopic analysis of 1111 FGK dwarfs observed within the context of the HARPS GTO planet search program. The paper is organized as follows: in Sect. 2, we introduce the sample used in this work. The method of the chemical abundance determination and analysis will be explained in Sect. 3. This section also includes discussion of the uncertainties and errors in our methodology as well as a comparison of our results with the literature. The calculation of the galactic space velocity data and the selection of different populations of stars, based on their kinematic and chemical properties, are presented in Sect. 4. A discussion of the [X/H] abundances of the exoplanet hosts can be found in Sect. 5. The main conclusions of the paper are finally addressed in Sect. 6. The extensive and full investigation of this sample, focused on the abundance difference between stars with and without planets will be presented in a parallel paper (Adibekyan et al. 2012).

2. Sample description and stellar parameters

The sample used in this work consists of 1111 FGK stars observed in the context of the HARPS GTO programs. It is a combination of three HARPS subsamples hereafter called HARPS-1 (Mayor et al. 2003), HARPS-2 (Lo Curto et al. 2010), and HARPS-4 (Santos et al. 2011). Note that the HARPS-2 planet search program is the complement of the previously started CORALIE survey (Udry et al. 2000) to fainter magnitudes and to a larger volume. The stars were selected to be suitable for radial velocity surveys. They are slowly rotating and non-evolved solar-type dwarfs with spectral type between F2 and M0 that do not show a high level of chromospheric activity either.

The individual spectra of each star were reduced using the HARPS pipeline and then combined with IRAF[2] after correcting for its radial velocity. The final spectra have a resolution of $R \sim 110\,000$ and signal-to-noise ratio (S/N) ranging from ~20 to ~2000, depending on the amount and quality of the original spectra. Fifty-five percent of the spectra have an S/N higher than 200, about 16% of stars have an S/N lower than 100, and less than 1% of the stars have an S/N lower than 40.

Precise stellar parameters for the entire sample were determined by Sousa et al. (2008, 2011a,b) using the same spectra as we did for this study. We refer the reader to these papers for details. The authors used a set of FeI and FeII lines whose equivalent widths (EW) were measured using the ARES[3] code (automatic routine for line equivalent widths in stellar spectra – Sousa et al. 2007)[4]. Assuming ionization and excitation equilibrium, the parameters were derived through an iterative process until the slope of the relation between the abundances given by individual FeI lines and both the excitation potential (χ_l) and reduced equivalent width ($\log EW/\lambda$) were zero, and until the FeI and FeII lines provided the same average abundance. The spectroscopic analysis was completed assuming local thermodynamic equilibrium (LTE) with a grid of Kurucz atmosphere models (Kurucz et al. 1993), and making use of a recent version of the MOOG[5] radiative transfer code (Sneden 1973). The typical precision uncertainties for the atmospheric parameters are of about 30 K for $T_{\rm eff}$, 0.06 dex for $\log g$, 0.08 km s^{-1} for $\xi_{\rm t}$, and 0.03 dex for [Fe/H]. We note that there are four stars in common between HARPS-1 and HARPS-4, and 14 stars between the HARPS-2 and HARPS-4 subsamples.

The stars in the sample have derived effective temperatures from 4487 K to 7212 K, but very few stars have temperatures that are very different from those of the Sun (there are e.g. only 12 stars with $T_{\rm eff} > 6500$ K). The metallicites of the stars range from –1.39 to 0.55 dex and have surface gravities from 2.68 to 4.96 dex (again there are very few "outliers", only five stars with $\log g < 3.8$ dex).

As already noted before, HARPS has contributed very much to the present high number of known planetary systems. Recently, Mayor et al. (2011) reported on the results of an eight-year HARPS survey with a statistical analysis of the planet and host samples. Simultaneously, they presented the list of newly discovered planets. We included these data when we updated the original GTO (Guaranteed Time Observations) catalog using data from the extra-solar planets encyclopedia[6]. The total number of PHSs in the current sample is now 135, of which 26 are super-Earths and Neptune-mass (the mass of the heaviest planet is less than 30 $M_\oplus$) planet hosts (hereafter NH).

3. Abundance analysis and uncertainties

Elemental abundances for 12 elements (Na, Mg, Al, Si, Ca, Ti, Cr, Ni, Co, Sc, Mn, and V) were determined using an LTE analysis with the Sun as reference point with the 2010 revised version of the spectral synthesis code MOOG (Sneden 1973) and a grid of Kurucz ATLAS9 plane-parallel model atmospheres (Kurucz et al. 1993). The reference abundances used in the analysis were taken from Anders & Grevesse (1989). The line list and atomic parameters of Neves et al. (2009) were used, adding the CaI line at λ5260.39 (excitation energy of the lower energy level $\chi_1 = 2.52$, and oscillator strength $\log gf = -1.836$) and excluding five NiI lines (λ4811.99, λ4946.04, λ4995.66, λ5392.33, and λ5638.75), two SiI lines (λ5517.54 and λ5797.87), two TiII lines (λ4657.20 and λ4708.67) and five TiI lines (λ4656.47, λ5064.06, λ5113.44, λ5219.70, and λ5490.16). These lines were excluded because the [X/Fe] abundance rations determined by them showed significant trends with effective temperature (see also Neves et al. 2009, for details of the lines selection). The EWs were automatically measured with the ARES code. The

[2] IRAF is distributed by National Optical Astronomy Observatories, operated by the Association of Universities for Research in Astronomy, Inc., under contract with the National Science Foundation, USA.

[3] The ARES code can be downloaded at http://www.astro.up.pt/sousasag/ares

[4] The *EW*s of the lines for the entire sample is available at the CDS.

[5] The source code of MOOG2010 can be downloaded at http://www.as.utexas.edu/~chris/moog.html

[6] http://exoplanet.eu/

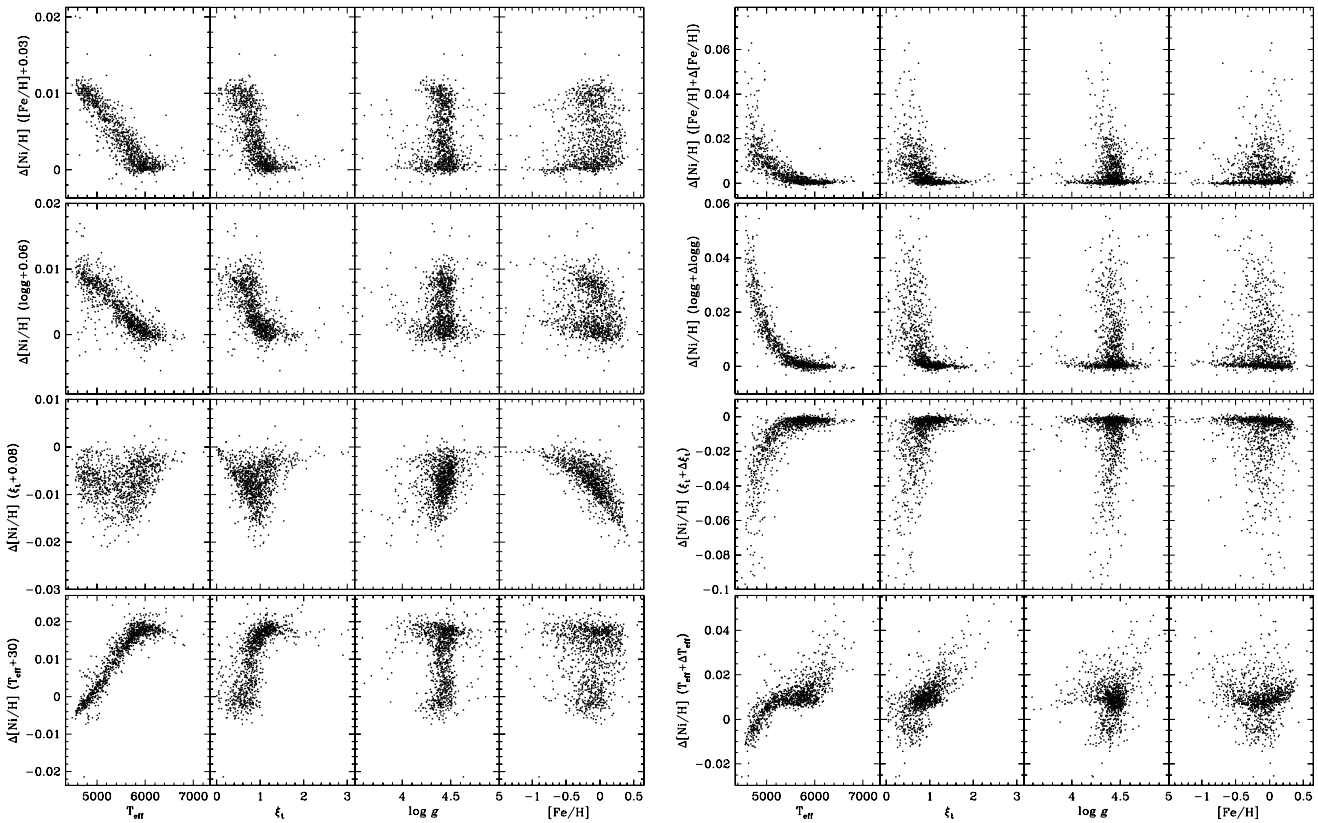

Fig. 1. Ni abundance sensitivity to the stellar parameter variations as a function of model atmosphere parameters. *Left* – The variation of the atmospheric parameters are the same for all stars and are equal to the typical errors. *Right* – The variation of the atmospheric parameters are equal to their one-sigma errors taken for each star individually.

input parameters for ARES were calculated following the procedure discussed in Sousa et al. (2011b).

The final abundance for each star and element was calculated to be the average value of the abundances given by all lines detected in a given star and element. Individual lines for a given star and element with a line dispersion more than a factor of two higher than the rms were excluded. In this way we avoided the errors caused by bad pixels, cosmic rays, or other unknown effects.

3.1. Uncertainties

Since the abundances were determined via the measurement of EWs and using already determined stellar parameters, the errors might still come from the EW measurements, from the errors in the atomic parameters, and from the uncertainties of the atmospheric parameters that were used to make an atmosphere model. In addition to the above-mentioned errors, one should add systematic errors that can occur due to NLTE or granulation (3D) effects. To minimize the errors, it is very important to use high-quality data and as many lines as possible for each element.

It is hard to define the contribution of each error source on the abundance results separately, but we can examine the sensitivity of the abundances to the stellar parameters and test the reliability of our results by comparing the abundances with those obtained in the literature.

First, to study the sensitivity trends of the abundances to the variation of the stellar parameters in general, we performed numerical tests with variations in the model parameters by a constant value similar to their typical errors: $\Delta T_{\rm eff}$ = ±30 K, $\Delta \log g$ = ±0.06 dex, $\Delta\xi_{\rm t}$ = ±0.08 km s^{-1}, and Δ[Fe/H] = ±0.03 dex. Then we calculated the abundance differences between the values obtained with and without varying the parameter. The maxima from the plus and minus cases were taken. A thorough investigation of this experiment shows that the picture is quite complicated. Changing one of the parameters will increase or decrease the abundance of a certain element depending on the stellar parameters. For example, in Fig. 1 (left panel) one can see that a variation of $T_{\rm eff}$ by +30 K may change the Ni abundance from about +0.02 to −0.01 dex, depending on the $T_{\rm eff}$ of the stars. Despite the complex picture, it can be observed that in general, the sensitivity of all element abundances to the stellar parameters also depends on the effective temperature. Following this correlation, we grouped our sample stars into three temperature groups: "low $T_{\rm eff}$" stars – stars with $T_{\rm eff} < 5277$ K, "*solar*" – stars with $T_{\rm eff} = T_{\odot} \pm 500$ K, and "high $T_{\rm eff}$" – stars with $T_{\rm eff} > 6277$ K. The average of the stellar parameters for the aforementioned groups are presnted in Table 1.

Table 1. Average of the stellar parameters for the subsamples with different $T_{\rm eff}$.

	$T_{\rm eff}$ (K)	log g (dex)	[Fe/H] (dex)	$\xi_{\rm t}$ (km s^{-1})
low $T_{\rm eff}$	4934	4.4	–0.17	0.59
Solar	5769	4.39	–0.12	1.01
high $T_{\rm eff}$	6440	4.51	–0.05	1.7

The results obtained from the test for three groups of stars are displayed in Table 2. Table 2 shows that neutral species are generally more sensitive to changes in effective temperature. For

Table 2. Abundance sensitivities of the studied elements to changes of ±100 K in $T_{\rm eff}$, ±0.2 dex in $\log g$ and [Fe/H], ±0.5 km s^{-1} in $\xi_{\rm t}$.

	FeI	NaI	MgI	AlI	SiI	CaI	ScI	ScII
$\Delta T_{\rm eff}$ = ±30 K								
low $T_{\rm eff}$	±0.00	±0.02	±0.01	±0.02	∓0.01	±0.03	±0.04	∓0.00
solar	±0.01	±0.01	±0.01	±0.01	±0.00	±0.02	±0.02	±0.00
high $T_{\rm eff}$	±0.01	±0.01	±0.01	±0.01	±0.01	±0.02	±0.02	±0.00
Δ[Fe/H] = ±0.03 dex								
low $T_{\rm eff}$	–	∓0.00	±0.00	±0.00	±0.01	±0.00	±0.00	±0.01
solar	–	±0.00	±0.00	±0.00	±0.00	±0.00	±0.00	±0.01
high $T_{\rm eff}$	–	±0.00	±0.00	±0.00	±0.00	±0.00	±0.00	±0.00
$\Delta \log g$ = ±0.06 dex								
low $T_{\rm eff}$	∓0.01	∓0.01	∓0.01	∓0.01	±0.01	∓0.02	∓0.01	±0.02
solar	∓0.01	∓0.00	∓0.01	∓0.00	±0.00	∓0.01	∓0.00	±0.02
high $T_{\rm eff}$	∓0.00	∓0.00	∓0.00	∓0.00	∓0.00	∓0.00	∓0.00	±0.02
$\Delta\xi_{\rm t}$ = ±0.08 km s^{-1}								
low $T_{\rm eff}$	∓0.01	∓0.00	∓0.00	∓0.00	∓0.00	∓0.01	∓0.01	∓0.01
solar	∓0.01	∓0.00	∓0.00	∓0.00	∓0.00	∓0.01	∓0.00	∓0.01
high $T_{\rm eff}$	∓0.00	∓0.00	∓0.00	∓0.00	∓0.00	∓0.01	∓0.00	∓0.01
	TiI	TiII	VI	CrI	CrII	MnI	CoI	NiI
$\Delta T_{\rm eff}$ = ±30 K								
low $T_{\rm eff}$	±0.04	∓0.00	±0.04	±0.03	∓0.02	±0.02	±0.00	±0.00
solar	±0.03	±0.00	±0.03	±0.02	∓0.00	±0.02	±0.02	±0.01
high $T_{\rm eff}$	±0.02	±0.00	±0.02	±0.02	∓0.00	±0.02	±0.02	±0.02
Δ[Fe/H] = ±0.03 dex								
low $T_{\rm eff}$	±0.00	±0.01	±0.00	±0.00	±0.01	±0.01	±0.01	±0.01
solar	±0.00	±0.01	±0.00	±0.00	±0.00	±0.00	±0.00	±0.00
high $T_{\rm eff}$	±0.00	±0.00	±0.00	±0.00	±0.00	±0.00	±0.00	±0.00
$\Delta \log g$ = ±0.06 dex								
low $T_{\rm eff}$	∓0.01	±0.02	∓0.01	∓0.01	±0.02	∓0.02	±0.01	±0.01
solar	∓0.00	±0.02	∓0.00	∓0.00	±0.02	∓0.01	±0.00	±0.00
high $T_{\rm eff}$	∓0.00	±0.02	∓0.00	∓0.00	±0.02	∓0.00	∓0.00	±0.00
$\Delta\xi_{\rm t}$ = ±0.08 km s^{-1}								
low $T_{\rm eff}$	∓0.02	∓0.01	∓0.02	∓0.01	∓0.01	∓0.01	∓0.01	∓0.01
solar	∓0.01	∓0.01	∓0.00	∓0.01	∓0.02	∓0.02	∓0.00	∓0.01
high $T_{\rm eff}$	∓0.00	∓0.01	∓0.00	∓0.00	∓0.02	∓0.01	∓0.00	∓0.00

gravity variations, the neutral species were hardly affected, and the variations become noticeable only for stars with low $T_{\rm eff}$, but the ionized species constantly varied by the same amount independently of the effective temperature. The ions are also more sensitive to metallicity changes than the neutral elements, although the sensitivity is not as significant as that for either $T_{\rm eff}$ and $\log g$. Finally, microturbulence variations led to only very small changes in most abundances (because many species are represented only by weak lines) and only few species are an exception.

Table 2 gives an overview of the elemental abundances variation with the variation of the stellar parameters, but not the uncertainties induced by the errors in the stellar parameters for our sample. The spectroscopic stellar parameters and metallicities were derived based on the equivalent widths of the FeI and FeII weak lines by imposing excitation and ionization equilibrium assuming LTE (e.g. Sousa et al. 2011b, and references therein). The errors obtained for the stars are typically very small, especially for stars similar to the Sun. This comes directly from the method itself because a differential analysis is performed with the Sun as reference. Stars that are significantly cooler or hotter than the Sun have larger intrinsic errors. To estimate the scale errors induced by uncertainties in the model atmosphere parameters, we varied the model parameters by an amount of their one-sigma errors available for each star and then we again divided our sample stars into three temperature groups as presented above. The average errors in the $T_{\rm eff}$ are 70, 24, and 45 K for cool, Sun-like, and hot star groups, respectively. The average errors in $\log g$ are 0.15, 0.03, and 0.05, in $\xi_{\rm t}$ – 0.3, 0.04, and 0.08, and in [Fe/H] – 0.04, 0.02, and 0.03 for the three groups, respectively. The right panel of Fig. 1 shows an example of the abundance variations with the variation of the stellar parameters against model parameters for Ni. From the figure it becomes clear that for stars with atmospheric parameters close to those of the Sun the uncertainties induced by the errors in the stellar parameters are very small (except for $\log g$). This is because both the abundance and stellar parameters are determined using an analysis with the Sun as reference point.

We evaluated the errors in the abundances of all elements [X/H], adding quadratically the line-to-line scatter errors and errors induced by uncertainties in the model atmosphere parameters. The line-to-line scatter errors were estimated as $\sigma/\sqrt{N}$, where σ is the standard deviation of N measurements (unfortunately, for some elements we were only able to select two or three lines). The average of $\sigma/\sqrt{N}$ and [X/H] errors for the three grouped stars are presented in Table 3. The table shows that the $\sigma/\sqrt{N}$ errors constitute the main part of the σ[X/H] total errors for the stars with $T_{\rm eff} = T_{\odot} \pm 500$ K. The atmospheric parameters were obtained from the FeI and FeII lines by iterating until the correlation coefficients between $\log \epsilon$(FeI) and χ_1, and between $\log \epsilon$(FeI) and $\log(W_\lambda/\lambda)$ were zero, and the mean abundance given by FeI and FeII lines were the same (e.g. Santos et al. 2004a; Sousa et al. 2008). This means that the parameters are interrelated, i.e., variation of one parameter will influence others. Hence, the total error could be slightly higher due to the

Table 3. The average error for the element abundances [X/H], and abundance ratios [X/Fe].

	Low $T_{\rm eff}$			*solar*			High $T_{\rm eff}$		
Elem	$\frac{\sigma}{\sqrt{N}}$	σ[X/H]	σ[X/Fe]	$\frac{\sigma}{\sqrt{N}}$	σ[X/H]	σ[X/Fe]	$\frac{\sigma}{\sqrt{N}}$	σ[X/H]	σ[X/Fe]
NaI	0.05	0.09	0.08	0.02	0.02	0.02	0.06	0.07	0.06
MgI	0.07	0.08	0.07	0.03	0.04	0.03	0.05	0.06	0.05
AlI	0.03	0.07	0.06	0.02	0.03	0.02	0.08	0.09	0.08
SiI	0.02	0.05	0.06	0.01	0.01	0.01	0.02	0.03	0.02
CaI	0.03	0.10	0.09	0.01	0.02	0.01	0.02	0.04	0.02
ScI	0.11	0.16	0.13	0.03	0.04	0.03	0.04	0.14	0.06
ScII	0.04	0.08	0.08	0.02	0.03	0.03	0.04	0.05	0.04
TiI	0.02	0.12	0.10	0.01	0.02	0.01	0.02	0.04	0.02
TiII	0.05	0.09	0.09	0.02	0.03	0.03	0.03	0.04	0.05
VI	0.07	0.16	0.14	0.02	0.03	0.02	0.05	0.07	0.05
CrI	0.02	0.08	0.07	0.01	0.02	0.01	0.02	0.03	0.02
CrII	0.07	0.11	0.10	0.03	0.03	0.03	0.03	0.05	0.05
MnI	0.05	0.10	0.08	0.03	0.04	0.03	0.04	0.05	0.04
CoI	0.03	0.06	0.04	0.02	0.03	0.02	0.05	0.06	0.05
NiI	0.01	0.04	0.03	0.00	0.01	0.01	0.01	0.03	0.02

described covariance terms (e.g. Johnson et al 2002; Cayrel et al. 2004; Lai et al. 2008).

The errors in the abundance ratios, [X/Fe], were determined taking into account the differences between the sensitivities of the resulting abundance ratios to changes in the assumed atmospheric parameters and the dispersion of the abundances from individual lines of each X element. Table 2 shows that, in general, the model changes (variation of stellar parameters) induce similar effects in the abundances of different elements and Fe, so that they partially cancel out in the ratio [X/Fe]. The average error for the element abundances [X/H] and abundance ratios [X/Fe] are presented in Table 3.

3.2. Testing the validity of the stellar parameters

As stated before, the chemical abundances of the elements were derived by completing an LTE abundance analysis with the Sun as reference point using EW measurements. To check the validity limit of the adopted methodology in terms of stellar parameter ranges, and to test the stellar parameters themselves, we tested our results in a variety of ways. First we calculated the slopes of the derived abundances of the considered lines as a function of the excitation potential (EP) of the NiI lines. We chose nickel because its lines cover a wide range of EPs. In this way, we verified whether the excitation equilibrium enforced on the FeI lines of every star was applicable to other species. In Fig. 2, we plot the slopes of EP obtained for each star against the stellar parameters. The figure shows that there are no discernible trends of EP with $\log g$ and [Fe/H], but there is a trend with $T_{\rm eff}$ and $\xi_{\rm t}$ (the $\xi_{\rm t}$ trend is just noticeable): cooler stars with $T_{\rm eff} \lesssim 5000$ K, which also have low microturbulence velocities, have a systematic bias away from the expected values.

Then, in Fig. 3 we plot the [CrI/CrII] and [TiI/TiII] as a function of the stellar parameters to ensure that the ionization equilibrium enforced on the FeII lines (Sousa et al. 2008) is acceptable to other elements. The figure shows that the aforementioned ratios gradually increase with decreasing $T_{\rm eff}$. Finally, plotting our abundance values of [X/Fe] as a function of the stellar parameters, we detect a significant trend for the $T_{\rm eff}$ plot, which is presented in Fig. 4. As seen in Fig. 4, Co and Al show a systematic trend with $T_{\rm eff}$ in all temperature ranges and TiI, ScI, V, CrII, and Na show a trend with $T_{\rm eff}$ in the low-temperature domain. The higher effective temperatures of the elements from

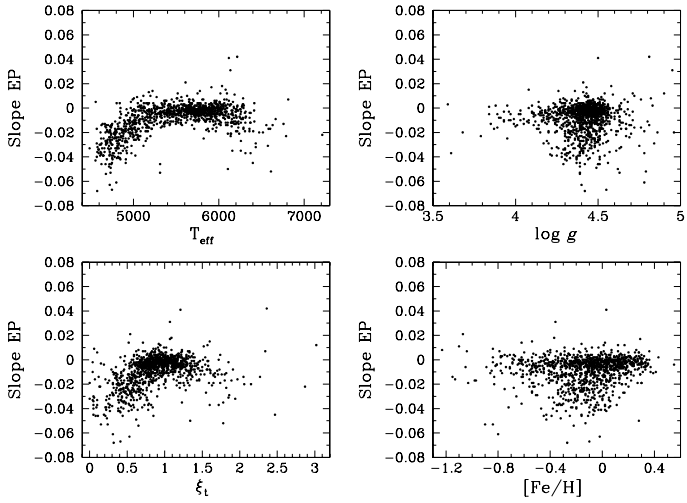

Fig. 2. Excitation potential slopes as a function of stellar atmospheric parameters for Ni.

which the trends appear are 4900 K for CrII, 5000 K for NaI and TiI, 5100 K for ScI and 5300 K for VI; these values are also indicated by vertical dotted lines in Fig. 4. As can be seen in Table 2, the elements and ions are very sensitive to the effective temperature, and the overestimation of the $T_{\rm eff}$ in the low-temperature domain might drift away from the expected abundance values. Similar trends for different elements with $T_{\rm eff}$ have been already noted in the literature (see e.g. Valenti & Fischer 2005; Preston et al. 2006; Gilli et al. 2006; Lai et al. 2008; Neves et al. 2009; Suda et al. 2011). As discussed in Neves et al. (2009), abundances of the cooler stars might have been overestimated due to the stronger line blending and also because the computed $\log gf$ values may be inadequate for these stars. The unexpected trends may also be connected to either deviations from excitation or ionization equilibrium, or to problems associated with the differential analysis. Finally, a possible explanation for the observed trends with $T_{\rm eff}$ could be an incorrect T-τ relationship in the adopted model atmospheres (Lai et al. 2008). While this effect on the derived [Fe/H] abundances can be compensated for by adjusting the value of the microturbulence, this does not apply to other elements.

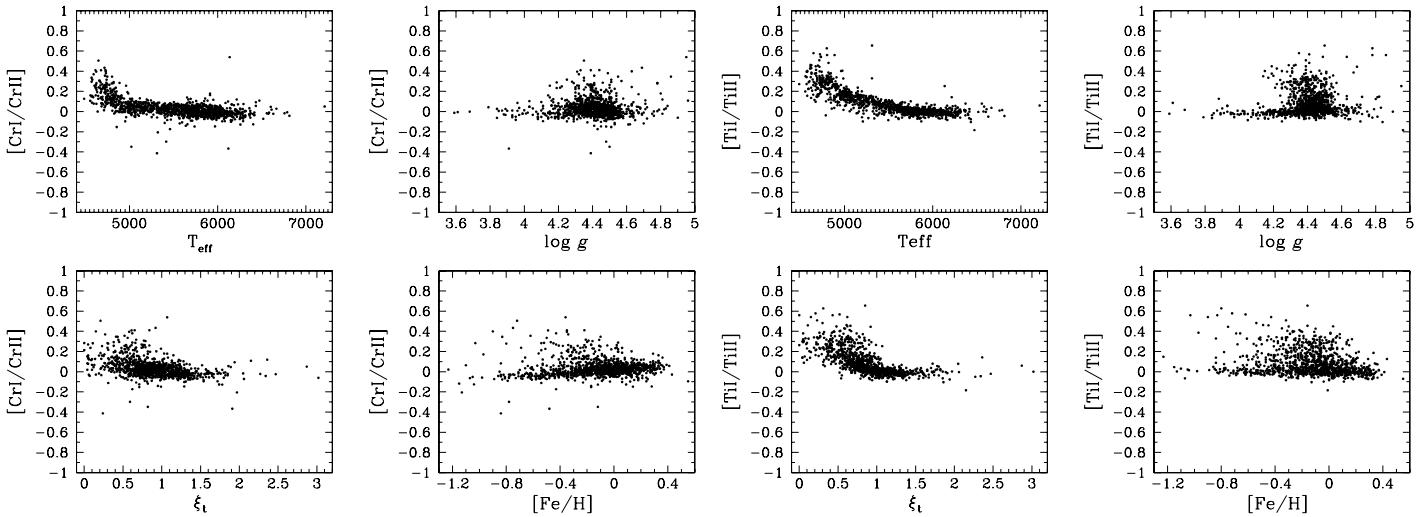

Fig. 3. [CrI/CrII] and [TiI/TiII] as a function of atmospheric parameters.

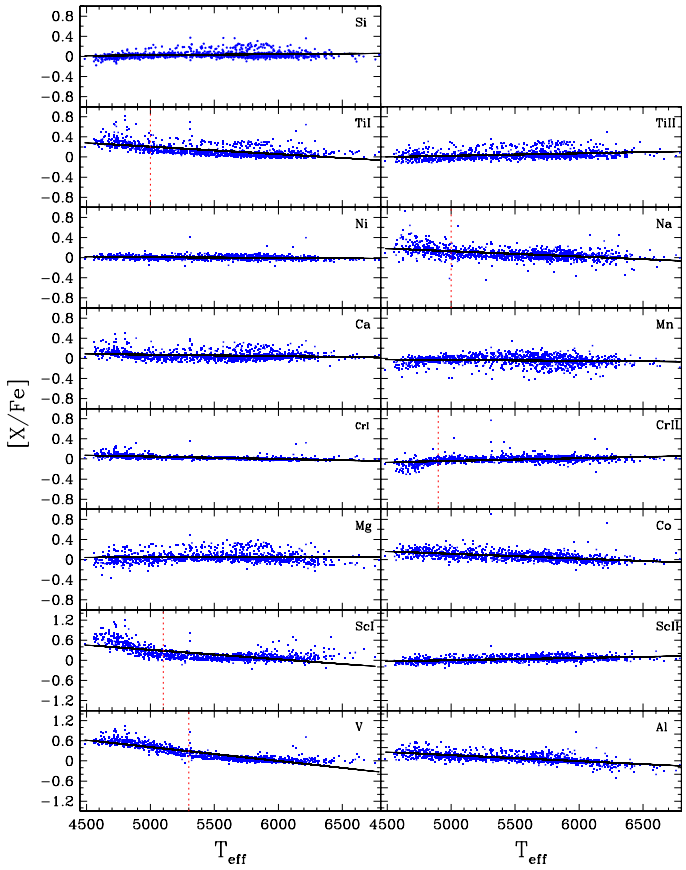

Fig. 4. [X/Fe] vs. $T_{\rm eff}$ plots. The blue dots represent the stars of the sample. The black solid lines depict the linear fits of the data. The vertical purple dotted lines indicate the "cutoff" temperature when [X/Fe] starts to show a systematic trend with $T_{\rm eff}$. Each element is identified in the *upper right corner* of the respective plot.

This discussion indicates that, the observed trends are probably not an effect of stellar evolution, and uncertainties in atmospheric models are the dominant effect in measurements. Therefore, we chose to remove the $T_{\rm eff}$ trends for these elements. We fitted the data by a cubic polynomial and adding a constant term, chosen so that the correction is zero at solar temperature. The constant term was added because simply subtracting the cubic would force the mean [X/Fe] to zero, which is an unphysical situation. A similar approach has already been applied in previous studies (see e.g. Valenti & Ficsher 2005; Petigura & Marcy 2011). A sample of our results for ten stars is presented in Table 4. We present the [X/H] values before and after correction for the $T_{\rm eff}$ trends. The complete results are available at the CDS.

3.3. Comparison with previous studies

As a final check of our method and analysis, we compare our derived abundances with those obtained by Bensby et al. (2005), Valenti & Ficsher (2005), Gilli et al. (2006), and Takeda (2007) for stars in common with this paper. Although we have 451 stars in common with Neves et al. (2009) and 270 with Delgado Mena et al. (2010), we do not present a comparisons of the abundances, because the methods, atomic data, and the line list are almost the same. Very small differences observed for individtheual stars and elements during the comparison with these papers can be explained with the small differences in the line list (see the beginning of Sect. 3) and moreover for some stars we used new spectra with higher S/N compared to those used in Neves et al. (2009). We note that the comparison was performed after removing the $T_{\rm eff}$ trends. The results are presented in Fig. 5. As can be seen, except for the paper by Gilli et al. (2006), our results agree very well with these previous studies which lends a certain reliability to our results. Figure 5 shows that there are systematic discrepancies with Gilli et al. (2006) for most of the elements. We note that Gilli et al. (2006) also observed systematic trends with $T_{\rm eff}$ for some at lower effective temperatures, but they did not correct their [X/Fe] abundance ratios. Our analysis shows that the higher discrepancies show stars with $T_{\rm eff} < 5000$ K. Unfortunately, we do not have cool stars ($T_{\rm eff} < 5000$ K) in common with Bensby et al. (2005), and Takeda (2007) to test an agreement (or disagreement) at low temperatures, but we have 15 cool stars in common with Valenti & Fischer (2005), whose abundance results agree very well with those achieved in this work. We note that Valenti & Fischer (2005) also observed abundance trends with $T_{\rm eff}$ for some elements, and as mentioned before, they chose to remove the spurious trends. The observed discrepancies with

Table 4. Sample table of the derived abundances of the elements, rms, and number of measured lines for each star.

Star	...	[TiI/H]	rms	n	[TiI/H]$_{corr}$*	[TiII/H]	rms	n	[VI/H]	rms	n	...
...	...	...	...	...	...	...	...	...	...	...	...	...
HD 109409	...	0.33	0.03	23	0.34	0.36	0.05	6	0.38	0.02	7	...
HD 109423	...	0.05	0.06	23	–0.06	–0.07	0.07	6	0.24	0.18	8	...
HD 109684	...	–0.27	0.05	24	–0.26	–0.24	0.03	6	–0.33	0.03	8	...
HD 109723	...	–0.01	0.06	25	–0.02	–0.10	0.03	6	0.00	0.06	8	...
HD 109988	...	0.23	0.05	23	0.14	0.15	0.07	6	0.53	0.20	8	...
HD 110291	...	0.03	0.05	23	–0.01	–0.03	0.05	6	0.08	0.07	8	...
HD 110557	...	0.04	0.04	23	–0.03	–0.05	0.04	6	0.17	0.15	8	...
HD 110619	...	–0.30	0.03	23	–0.31	–0.35	0.02	6	–0.35	0.01	8	...
HD 110668	...	0.16	0.05	23	0.16	0.22	0.01	5	0.22	0.04	8	...
HD 111031	...	0.30	0.03	24	0.30	0.29	0.03	6	0.35	0.02	7	...
...	...	...	...	...	...	...	...	...	...	...	...	...

Notes. (*) The [X/H] abundances after correction for the $T_{\rm eff}$ trends. The full table is available at the CDS.

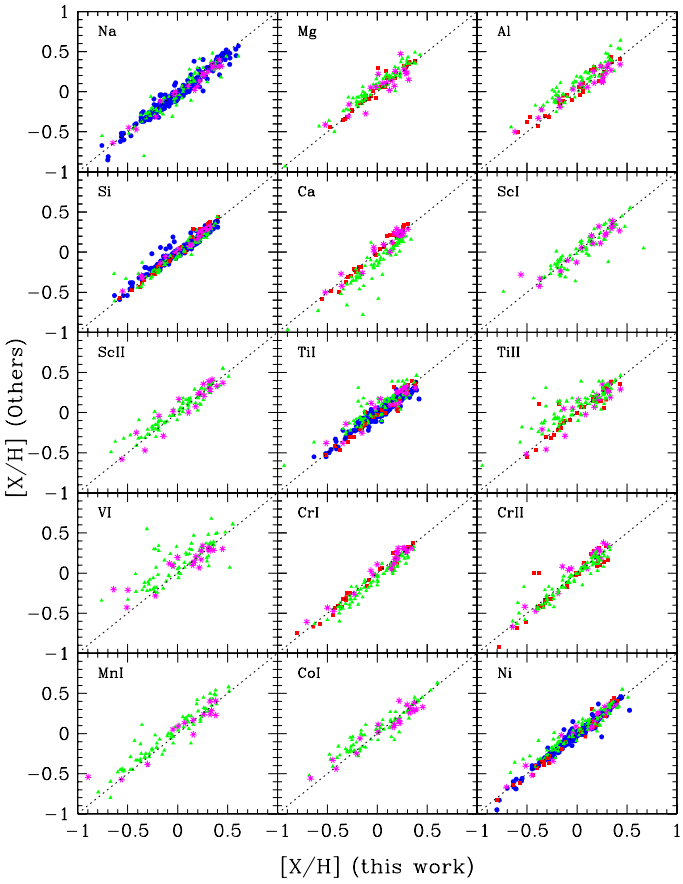

Fig. 5. Comparison of our abundance to those derived in other studies: Bensby et al. (2005) (red squares), Valenti & Fischer (2005) (blue dots), Gilli et al. (2006) (green triangles), and Takeda (2007) (magenta asterisks). The element label is located at the *upper left corner* of each plot.

Gilli et al. (2006) and at the same time perfect agreement with other studies confirm that applying corrections to remove the observed trends with $T_{\rm eff}$ is a correct approach.

4. Kinematics, chemistry, and stellar populations

The Milky Way (MW) has a composite structure with several stellar subsystems. The main three stellar populations of the MW in the solar neighborhood are the thin disk, thick disk, and the halo, although most of the stars belong to the thin disk. These populations have different kinematic and chemical properties. Generally, the thick disk is composed of relatively old (e.g. Bensby et al. 2005; Adibekyan et al. 2011), metal-poor and α-enhanced (Fuhrmann 1998; Prochaska et al. 2000; Feltzing et al. 2003; Mishenina et al. 2004; Reddy et al. 2006; Haywood 2008b; Lee et al. 2011) stars that move in Galactic orbits with a large-scale height and long-scale length (Robin et al. 1996; Buser et al. 2001; Jurić et al. 2008). However, recent analyses of the geometric decompositions of the Galactic disk based on the elemental-abundance selection of the sample stars yielded strikingly different results (see e.g., Bovy et al. 2012a,b; Liu & van de Ven 2012). The latter authors found a chemo-orbital evidence that the thicker component of the MW disk is not distinct from the thin component (the MW has no thick disk – Bovy et al. 2012a), which can be explained by smooth internal evolution through radial migration (Liu & van de Ven 2012). The exceptions are the old metal-poor stars with different orbital properties that could be part of a distinct thick-disk component formed through an external mechanism (Liu & van de Ven 2012).

The first and important step in developing an understanding of the differences between the thin (thinner) and the thick (thicker) disks is to find an accurate and reliable method of assigning a star to a certain population. There is no obvious predetermined way to identify purely thick or thin disk stars in the solar neighborhood. The main essential ways of distinguishing local thick and thin disk stars are a purely kinematical approach (e.g. Bensby et al. 2003, hereafter B03, 2005; Reddy et al. 2006), a purely chemical method (e.g. Navarro et al. 2011; Adibekyan et al. 2011), and looking at a combination of kinematics, metallicities, and stellar ages (e.g. Fuhrmann 1998; Haywood 2008a).

Although the kinematic selection is a much more common method than the chemical approach, the chemical distinction of the disks can be more useful and reliable, because chemistry is a relatively more stable property of a star than the spatial positions and kinematics. In this section we present the adopted methods to separate stars into different stellar populations on the basis of their chemistry and kinematics.

4.1. Kinematical separation

To separate different stellar population by their kinematics, we computed Galactic space velocities for the stars. The space velocity components (UVW) were derived with respect to the local standard of rest, adopting the standard solar motion ($U_\odot$, $V_\odot$, $W_\odot$) = (11.1, 12.24, 7.25) km s^{-1} of Schönrich et al. (2010). The main source of the parallaxes and proper motions were the

Table 5. Sample table of the Galactic space velocity components and the probabilities to assign the stellar population to which each star belongs.

Star	U_{LSR}	V_{LSR}	W_{LSR}	B03				R03			
				P_{thick}	P_{thin}	P_{halo}	group	P_{thick}	P_{thin}	P_{halo}	group
...	...	...	...	...	...	...	...	...	...	...	...
HD 104800	122	–131	–57	0.91	0.00	0.09	thick	0.84	0.00	0.16	thick
HD 104982	72	–10	–38	0.28	0.72	0.00	thin	0.13	0.87	0.00	thin
HD 105004	–34	–225	–76	0.00	0.00	1.00	halo	0.06	0.00	0.94	halo
HD 105671	–21	0	–8	0.01	0.99	0.00	thin	0.01	0.99	0.00	thin
HD 105779	–29	–37	7	0.03	0.97	0.00	thin	0.02	0.98	0.00	thin
HD 105837	23	13	41	0.15	0.85	0.00	thin	0.08	0.92	0.00	thin
HD 105938	35	0	13	0.02	0.98	0.00	thin	0.01	0.99	0.00	thin
HD 106116	–107	8	39	0.76	0.24	0.00	thick	0.29	0.71	0.00	thin
HD 106275	18	–69	11	0.38	0.62	0.00	trans	0.11	0.89	0.00	thin
HD 104006	–21	–188	1	0.48	0.00	0.52	trans	0.69	0.00	0.31	trans
...	...	...	...	...	...	...	...	...	...	...	...

Notes. The full table is available at the CDS.

updated version of the Hipparcos catalog (van Leeuwen 2007). Data for eight stars with unavailable Hipparcos information were taken from the TYCHO Reference Catalog (Hog et al. 1998). The parallaxes with errors larger than 10%, (which is true for less than 5% of the stars in the sample) were redetermined following the procedure described in Sousa et al. (2011b). The percentage of stars with inaccurate proper motions (errors larger than 10%) is less than 8%. We did not perform a quality selection of them, because these errors in general do not change their membership to a certain population. The radial velocities were obtained from the HARPS spectra (courtesy of the HARPS GTO team). Combining the measurement errors in the parallaxes, proper motions, and radial velocities, the resulting average errors in the U, V, and W velocities are of about 1 km s^{-1}.

The selection of the thin disk, thick disk, and halo stars was completed using the method described in Reddy et al. (2006). This assumes that the sample is a mixture of the three populations and each population follows a Gaussian distribution of random velocities in each component (Schwarzschild 1907). Here, we adopted the mean values (asymmetric drift) and dispersion in the Gaussian distribution (characteristic velocity dispersion), and the population fractions were taken from B03 and Robin et al. (2003, hereafter R03; see also Ojha et al. 1996; Soubiran et al. 2003). We considered that a probability in excess of 70% suffices to assign a star to the concrete population. All remaining stars with a probability of less than 70% were included in a transition population. A sample of the probabilities calculated for each star according to B03 and R03, as well as Galactic space velocity components used in their calculation, are presented in Table 5. The complete results are available at the CDS.

According to the B03 criteria, among the 1111 stars in our sample, we have 964 stars from the thin disk, 78 from the thick disk, 58 are considered to be transition stars that do not belong to any group, and only 11 star belong to the halo. Adopting the criteria from R03 gives 1016 thin disk stars, 49 thick disk stars, 36 transition stars, and 10 stars belonging to the halo. We note that the B03 criteria approximately translate into the R03 criteria if $P_{thick} > 50\%$ for a star to belong to the thick disk (Reddy et al. 2006). The distribution of stars of our sample in the Toomre diagram is shown in Fig. 6 using both the R03 and B03 criteria.

4.2. Chemical separation

As mentioned above, in addition to the difference in their kinematics and ages, the thin- and thick disk stars are also different in their α content at a given metallicity ([Fe/H]). This dichotomy in the chemical evolution allows one to separate different stellar populations.

Adibekyan et al. (2011) showed that the stars of our sample fall into two populations, clearly separated in terms of [α/Fe] ("α" refers to the average abundance of Mg, Si, and Ti) up to super-solar metallicities. We recall that Ca was not included in the α index, because at solar metallicities the [Ca/Fe] trend differs from that of other α-elements. In turn, high-α stars were also separated into two families with a gap in both [α/Fe] ([α/Fe] $\approx$ 0.17) and metallicity ([Fe/H] ≈ -0.2) distributions. This showed that the metal-rich high-α stars (hαmr) and metal-poor high-α (thick disk) stars are on average older than chemically defined thin disk stars (low-α stars). At the same time hαmr stars have kinematics and orbits similar to the thin disk stars.

Although in Adibekyan et al. (2011) we established a cutoff temperature for TiI because of the observed trend with T_{eff} for the [TiI/Fe] ratio (here we removed these trends, which are also observed for some other elements, see Sect. 3.2), the chemical separation of the stellar population was based on the stars with effective temperatures close to the Sun by ±300 K. In this paper we used the chemical separation described in Adibekyan et al. (2011), i.e., thin disk, thick disk, and hαmr stars.

The [α/Fe] versus [Fe/H] plot for the sample stars is depicted in Fig. 7. The blue triangles refer to the thick disk, red circles to the thin disk. The green asterisks and the black crosses refer to the transition stars between thin-thick and thick-halo, respectively. Magenta squares represent the stars belonging to the halo. For the kinematical separation in the top panel we used the criteria from R03, and in the bottom panel the stars are separated according to the B03 criteria. The black dashed curve separates the stars with high- and low-α content. Clearly, the kinematically selected samples of thick- and thin disk stars are both well mixed, judging by their [α/Fe]. The chemically separated thin disk contains several kinematically hot stars that are classified as thick disk stars. Using the R03 criteria almost "cleans" the thin disk from the kinematically selected thick disk stars, but produces a high "contamination" of the chemically selected thick disk by stars with thin disk kinematics. This mixing and contamination must in part result from the fact that the assignment to the thin or the thick disk is based on probability, but the main reason could be that the stars in the local neighborhood have different birth radii and reached the solar neighborhood because of their eccentric orbits or via radial migration (e.g. Haywood 2008b; Schönrich & Binney 2009).

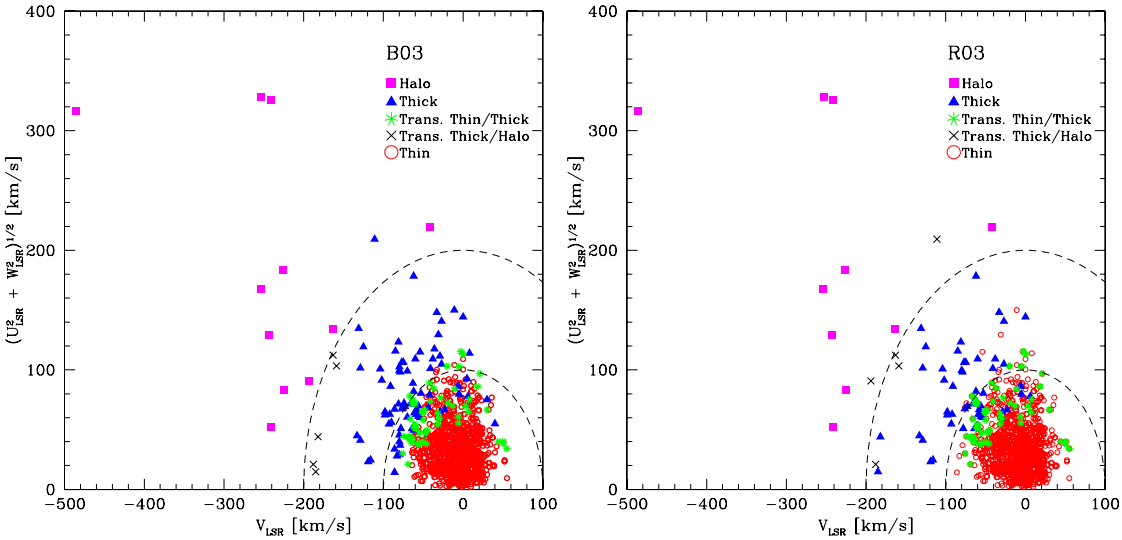

Fig. 6. Toomre diagram for the entire sample. The *left and right* panels show the separation of the stellar groups according to the B03 and R03 criteria, respectively. The symbols are explained in the figure.

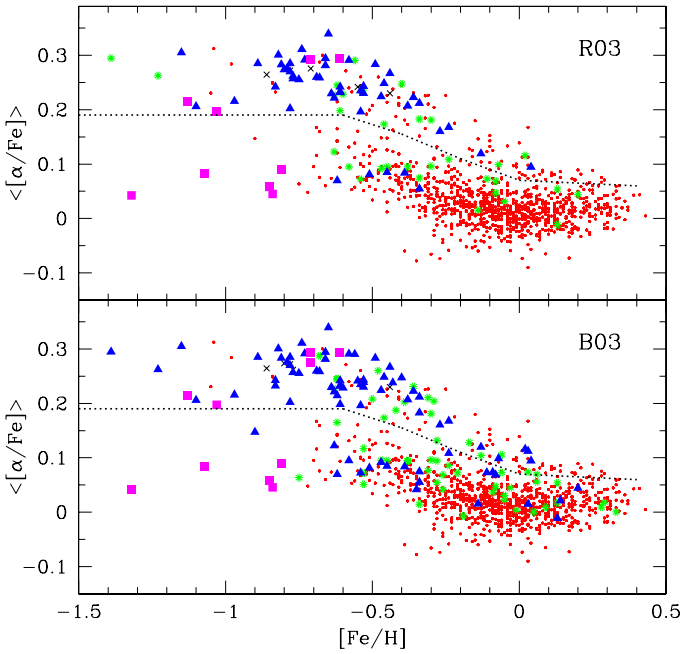

Fig. 7. Abundance ratios [α/Fe] vs. [Fe/H] for the total sample. The blue triangles refer to the thick disk, red circles to the thin disk. The green asterisks and the black crosses refer to the transition stars between thin-thick and thick-halo, respectively. Magenta squares represent the stars belonging to the halo. The black dashed curve separates the stars with high- and low-α content.

4.3. The [X/Fe] vs. [Fe/H]: the thin- and thick disks

Low-mass stars have long lifetimes and their envelopes have preserved much of their original chemical composition. Studying FGK dwarfs is very useful because they contain information about the history of the evolution of chemical abundances in the Galaxy. The [X/Fe] vs. [Fe/H] is traditionally used to study the Galactic chemical evolution because iron is a good chronological indicator of nucleosynthesis. In this paper we will not describe the [X/Fe] abundance trends relative to Fe because they are discussed in Neves et al. (2009), whose sample consisted of about half the number of our stars. Neves et al. (2009) also performed a detailed analysis of the [X/Fe] distributions of the kinematically separated stellar populations. In this subsection we will discuss how the chemically separated stellar families are similar or different from each other in terms of their [X/Fe].

In Fig. 8 we show the [X/Fe] abundance trends relative to [Fe/H] for the stars with $T_{\rm eff} = T_{\odot} \pm 300$ K. In the plot we present only stars with temperatures close to those of the Sun, because the abundance determinations for these stars are more accurate and allow us to avoid overloading the plot to obtain a clearer picture of the trends in the stellar groups. The corresponding figure for the total sample is shown in Fig. A.1. The blue circles and black dots refer to the chemically selected thick- and thin disk stars, and the red filled triangles represent the hαmr stars. Magenta squares are the stars belonging to the halo according to their kinematics. In the plot we used the average of TiI & TiII for Ti, the average of CrI & CrII for Cr, and the average of ScI & ScII for Sc to increase the statistics. The abundance trends do not change when using the mean values as compared to using the different ions separately. There is, however, lower scatter in the plots when the average values are used. It is difficult to say whether the heavy scatter found in some plots is astrophysical or due to errors.

González Hernández et al. (2010) noted the low dispersion of most of the elements received for their sample of solar twins and analogs with $S/N > 350$. To understand if the higher scatter found in this work is due to the quality of the data, we created a sample of solar analogs with the same stellar parameters as described in González Hernández et al. (2010). Then we devided the sample into two subsamples with $S/N > 400$ and $S/N < 150$. In general, we found similar dispersions for the two subsamples, comparable with those found in González Hernández et al. (2010).

Figure 8 shows that in addition to the Mg, Si, and Ti (on which our chemical separation is based), the thin- and thick disks are chemically different for Al, Sc, Co, and Ca. There are some hints that the two disks have different Na, V, Ni, and Mn ratios, but there is no clear boundary of their [X/Fe] ratios. The only element for which the thin and the thick disks have the same [X/Fe] values is Cr. A similar result was obtained in Neves et al. (2009), who separated the thin- and thick disks according to the kinematical features of the stars.

Inspection of Fig. 8 shows that the α-enhanced families, separated from the thick disk by the α-element and Fe content, show different [X/Fe] trends with metallicity for different elements. As can be seen, at metallicities above solar the thin disk stars show a rise in the [Al/Fe], [Sc/Fe], [V/Fe], [Ni/Fe] [Co/Fe], and

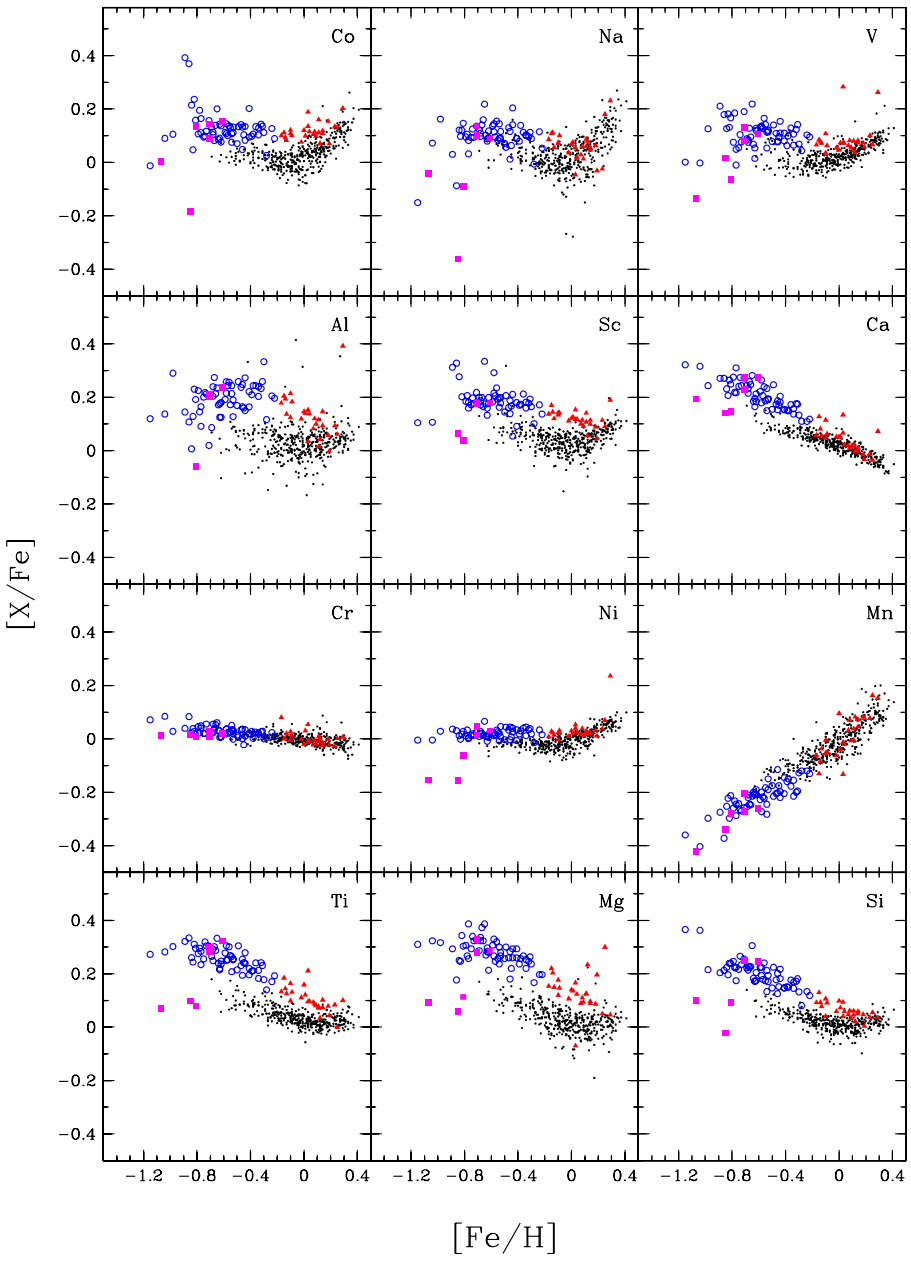

Fig. 8. Abundance ratios [X/Fe] vs. [Fe/H] for the stars with $T_{\rm eff} = T_{\odot} \pm 300$ K. The blue circles and black dots refer to the chemically selected thick- and thin disk stars, and the red filled triangles are the hαmr stars. Each element is identified in the *upper right corner* of the respective plot. Magenta squares represent the stars belonging to the halo according to their kinematcs. The total sample is shown in Fig. A.1.

[Na/Fe] (for the last two elements the rise is more pronounced and steeper), while the [Sc/Fe], [Co/Fe], [Ni/Fe], and [V/Fe] trends for the hαmr stars are essentially flat; moreover, for the [Na/Fe] and [Al/Fe] we observe a downward trend. It is interesting to see that the hαmr group stars are mixed with the thin disk stars in the [Ca/Fe] vs. [Fe/H] plot, while the thick- and thin disks are separated well.

Adibekyan et al. (2011), studying the orbital properties and α-element abundances of these stars, have put forward the idea that this group of stars may have originated from the inner Galactic disk. Nevertheless, their origin and exact nature still remains to be clarified.

5. [X/H] of planet-host stars

As stated before, in a separate paper we will focus on the the abundance differences between the stars with and without planets. In this section we will briefly describe the sample of planet-host and non-host stars in terms of their [X/H].

The strong correlation is now well established between the rate of giant planets and host star metallicity. In turn, as noted before, recent studies showed that Neptune and super-Earth class planet hosts have a different metallicity distribution compared to those with giant gaseous planets. Although in this study we used relatively few PHSs (109 hosts of giants, and 26 hosts of only Neptune masses and below), this number is sufficient to observe whether there are any discernible differences in the abundances of stars without planets and planets with different masses. The [X/H] distribution histograms for planet- and non-planet hosts are depicted in Fig. 9. The stars with giant planets, without planets, and the stars hosting exclusively Neptunes and super-Earths are represented by a dashed red, dotted black, and shaded blue line, respectively.

As expected, we observe a clear metallicity excess for Jovian hosts (JH) in all spaces, which agrees well with previ-

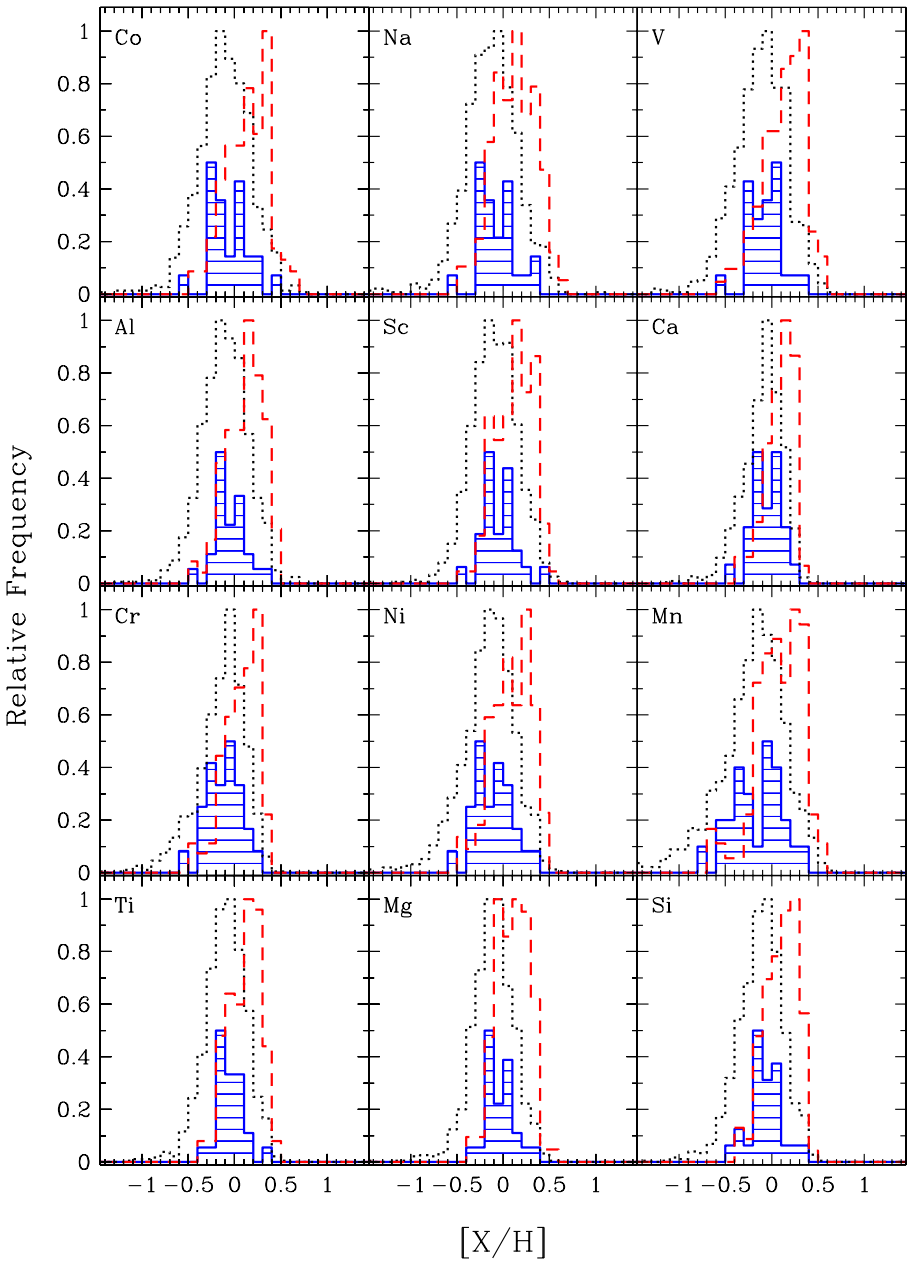

Fig. 9. [X/H] distribution of the different elements. The stars with giant planets and without planets are represented by a red dashed and black dotted lines, respectively. The stars that exclusively host Neptunian and super-Earth planets are represented by a shaded blue. The Neptunian and super-Earth distribution was set smaller for clarity. The element label is located at the *upper left corner* of each plot.

ous similar studies for refractory elements (e.g. Bodaghee et al. 2003; Gilli et al. 2006; Takeda et al. 2007; Neves et al. 2009; Kang et al. 2011) and for iron (e.g. Gonzalez et al. 2001; Santos et al. 2001, 2003, 2004a, 2005; Fischer & Valenti 2005; Bond et al. 2006, 2008; Johnson et al. 2010). As already noted in the literature (e.g. Gilli et al. 2006; Neves et al. 2009), in most histograms the distributions of the abundances in JHs are not symmetrical: the distribution increases with [X/H] to a maximum value and afterward abruptly drops. The observed cutoff might suggest that this is the metallicity limit of solar neighborhood stars (e.g. Santos et al. 2003), since most of the planet hosts are at the high-metallicity end of the sample.

As can be seen from Fig. 9, the [X/H] distribution of 26 NHs in general repeats the distribution of stars without planets for all elements we studied (except that the distributions start very abruptly from the metal-poor side, probably indicating the minimum amount of some metals required to form them). This result confirms the "metal-poor" nature (e.g. Udry & Santos 2007; Sousa et al. 2008, 2011a; Mayor et al. 2011) of low-mass planet hosts, when extended to elements other than iron. The average values of [X/H] for three groups of stars, along with their rms dispersion, the number of stars used in their determination, and the difference of averages between Neptunian and Jovian hosts and stars without planets are listed in Table 6. These differences range from 0.17 (CaI) to 0.28 (MnI) for JHs and from 0.01 (CrII) to 0.09 (MgI) for NHs. These values agree well with those obtained by Neves et al. (2009) for the sample of 451 FGK stars.

Figure 10 illustrates the fraction of stars with Neptune-like and gaseous giant planets as a function of [X/H]. For each bin (the size of each bin is 0.1 dex), we divided the number of planet-bearing stars by the total number of stars in the bin. For all elements studied, we observe a continuous increase in the percentage of JHs as a function of increasing [X/H]. This result agrees with the previous findings of other authors e.g. Santos et al. (2001), Fischer & Valenti (2005), and Neves et al. (2009) for [Fe/H] and Petigura & Marcy (2011) for [O/H], [C/H] and [Fe/H]. Petigura & Marcy (2011), noting the small-number statistics, reported a hint of possible plateau or turnover at the

Table 6. Average abundances [X/H] for stars without planets, with giant planets, and stars that exclusively host Neptunians, along with their rms dispersion, the number of stars used in their determination, and the difference of averages between Neptunian and Jovian hosts and stars without planets.

Species	Jovian hosts			Neptunian hosts			Non-planet hosts			Difference of Averages	
X	⟨[X/H]⟩	σ	N	⟨[X/H]⟩	σ	N	⟨[X/H]⟩	σ	N	Jovian – Non-hosts	Neptunian – Non-hosts
NaI	0.12	0.23	109	–0.06	0.21	26	–0.12	0.30	975	0.24	0.06
MgI	0.10	0.18	109	–0.02	0.14	26	–0.11	0.23	976	0.21	0.09
AlI	0.10	0.19	109	–0.04	0.16	26	–0.11	0.25	969	0.21	0.07
SiI	0.10	0.18	109	–0.07	0.17	26	–0.12	0.24	976	0.22	0.05
CaI	0.08	0.15	109	–0.05	0.15	26	–0.09	0.21	976	0.17	0.04
ScI	0.14	0.21	109	–0.01	0.18	26	–0.08	0.25	947	0.22	0.07
ScII	0.11	0.20	109	–0.06	0.19	26	–0.12	0.27	976	0.23	0.06
TiI	0.11	0.17	109	–0.03	0.14	26	–0.08	0.22	976	0.19	0.05
TiII	0.10	0.18	109	–0.07	0.16	26	–0.11	0.23	976	0.21	0.04
VI	0.13	0.22	109	–0.06	0.19	26	–0.11	0.28	973	0.24	0.05
CrI	0.08	0.19	109	–0.09	0.18	26	–0.13	0.26	976	0.21	0.04
CrII	0.05	0.18	109	–0.14	0.18	26	–0.15	0.26	976	0.20	0.01
MnI	0.08	0.25	109	–0.17	0.27	26	–0.20	0.35	976	0.28	0.03
CoI	0.13	0.23	109	–0.06	0.20	26	–0.11	0.28	975	0.24	0.05
NiI	0.09	0.21	109	–0.10	0.21	26	–0.16	0.30	976	0.25	0.06
FeI	0.07	0.19	109	–0.12	0.2	26	–0.16	0.27	976	0.23	0.04
$\log g$	4.37	0.14	109	4.39	0.08	26	4.41	0.15	976	–0.04	–0.02
ξ_t	1.01	0.25	109	0.81	0.23	26	0.88	0.37	976	0.13	–0.07
$T_{\rm eff}$	5656	412	109	5442	359	26	5490	502	976	166	–48

Notes. The four bottom rows list the average stellar parameters of the three aforementioned groups, taken from Sousa et al. (2008, 2011a,b).

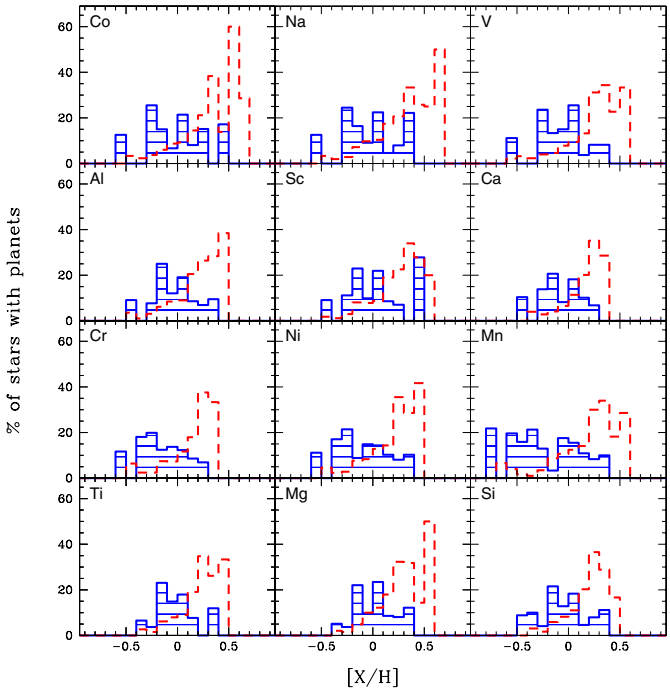

Fig. 10. Percentage of stars with giant (dashed red) and exclusively Neptunian and super-Earth (shaded blue) planets as a function of [X/H]. The Neptunian and super-Earth distribution was multiplied by 5 for clarity. Each element is identified in the *upper left corner* of the respective plot.

highest abundance bins for [C/H] and [Fe/H]. For our sample stars it is also possible to observe a small plateau or even turnover for some elements (Si, Ca, Sc, V, Cr, and Mn), but we also should note that at the highest abundance bins the number of stars sometimes does not exceed 4–5 stars.

For the fraction of low-mass planets hosts we do not observe any increasing or decreasing trends with [X/H] abundances. The distributions of the percentage of NHs are in general symmetric around the mean values listed in Table 6, which are on average less than solar abundance values by about 0.05 dex. These observations agree with the previous results for [Fe/H] (e.g. Sousa et al. 2008; Ghezzi et al. 2010; Mayor et al. 2011).

When we consider the possible dependence of planet formation on chemical composition, Gonzalez (2009) recommended to use a so-called refractory index "Ref", which quantifies the mass abundances of refractory elements (Mg, Si and Fe) important for planet formation, rather than [Fe/H]. The importance of this index increases in the Fe-poor region, when one compares statistics of planets around the thin disk and thick disk stars. The left panel of Fig. 11 illustrates the [Fe/H] and [Ref/H] distribution histograms for planet and non-planet host stars. The fraction of stars with planets of different mass as a function of [Fe/H] and [Ref/H] are presented in the right panels. Clearly, the distributions of the three subsamples are shifted toward the higher "metallicities" in the [Ref/H] histograms, compared to their distributions in the [Fe/H]. This shift in the redistribution for planet-host stars is higher at lower metallicities, indicating their high [α/Fe] values. We again observe turnover at the highest abundance bins for [Fe/H] and [Ref/H].

The four bottom rows in Table 6 list the average stellar parameters of the three groups. It shows that hosts of low-mass planets on average have the same effective temperature as non-host stars. Interestingly, JHs are hotter by about 170 K than their non-host counterparts. The planet-search surveys are usually based on volume-limited samples, but the criteria to "cut" the sample were usually also based on the $B-V$ color. Our sample stars mostly have $B-V$ colors from 0.5 to 1.2. The top panel in Fig. 12 shows our sample stars in the [Fe/H] against $T_{\rm eff}$ (note that one star with $T_{\rm eff}$ = 7212 K is not presented in the plot). The dotted lines represent the approximate lower and upper limits in $B-V$ ($B-V$ = 0.5 and 1.2). The lines were constructed using

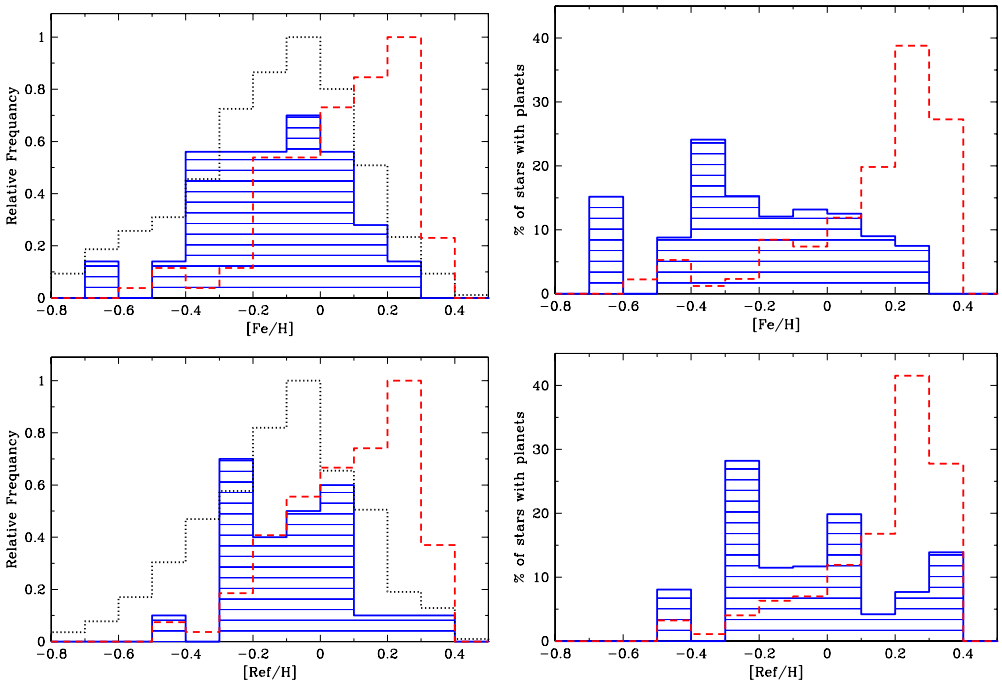

Fig. 11. *Left* – [Fe/H] and [Ref/H] distribution of the sample stars. The distribution lines for Jovian, Neptunian/super-Earth host and non-host stars are the same as in Fig. 9. The Neptunian and super-Earth distribution was set smaller for clarity. *Right* – Percentage of stars with giant (red dashed) and exclusively Neptunian and super-Earth (shaded blue) planets as a function of [Fe/H] and [Ref/H]. The Neptunian and super-Earth distribution was multiplied by 5 for better visibility.

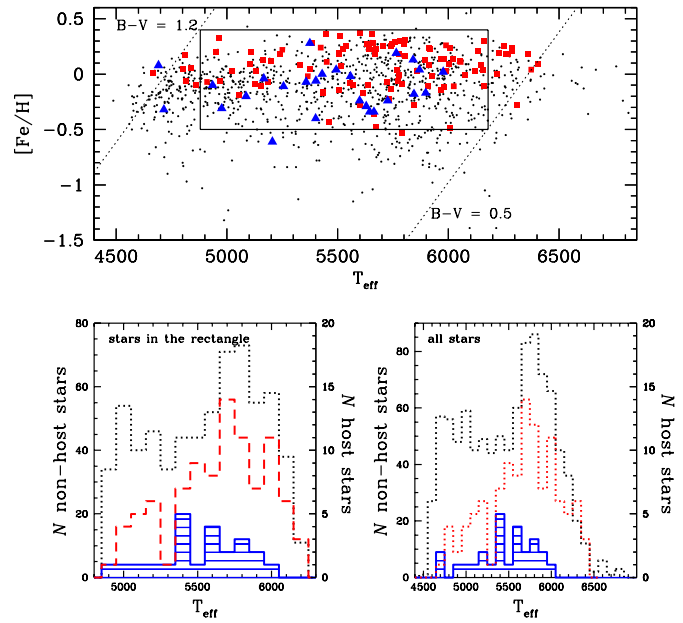

Fig. 12. Metallicity as a function of the effective temperature for stars with Jupiters (red circles), with Neptunes (blue triangles) and comparison sample stars (black crosses). The dotted line represents the approximate lower and upper limits in $B-V$ ($B-V$ = 0.5 and 1.2). The $T_{\rm eff}$ distributions of all sample stars without planets (black dotted) and stars hosting Jovians (red dashed) and only Neptunians (shaded blue) are presented in the right bottom panel, and the distributions of the stars in the rectangle are shown in the *left bottom*.

the calibration equation from Sousa et al. (2008). Evidently, we missed stars with "low" [Fe/H] and "high" $T_{\rm eff}$ in our sample, as well as "high" [Fe/H] objects with "low" $T_{\rm eff}$. To avoid these biases in [Fe/H] and $T_{\rm eff}$, we cut our sample in [Fe/H] and in $T_{\rm eff}$, as shown in Fig. 12. The $T_{\rm eff}$ distributions of all sample stars without planets and stars hosting Jovians and only Neptunians are presented in the right bottom panel of Fig. 12, and the distributions of the same groups of stars lying in the "cut rectangle" are shown in the left. The difference of average $T_{\rm eff}$s of Jupiter hosts and non-host stars in the rectangle has now decreased, reaching about 80 K, and for NHs about 50 K. We note that the observed low bimodality in $T_{\rm eff}$ for all three groups (with a minimum in $T_{\rm eff} \approx 5300$ K) are inherited from the Hipparcos catalog (see e.g. Ammons et al. 2006, for the $T_{\rm eff}$ distribution of Hipparcos stars), on which the HARPS sample is based.

The three groups of stars have on average almost the same $\log g$. The difference in $\xi_{\rm t}$ reflects the difference in $T_{\rm eff}$, as discussed above. The [Fe/H] distributions of stars with and without planets are already extensively discussed in Sousa et al. (2008, 2011a,b).

6. Concluding remarks

We have carried out a uniform abundance analysis for 12 refractory elements (Na, Mg, Al, Si, Ca, Ti, Cr, Ni, Co, Sc, Mn, and V) for a sample of 1111 FGK dwarf stars from the HARPS GTO planet search program. Of these stars, 135 are known to harbor planetary companions (26 of them are exclusively hosting Neptunians and super-Earth planets) and the remaining 976 stars do not have any known orbiting planet. The precise spectroscopic parameters for the entire sample were derived by Sousa et al. (2008, 2011a,b) in the same manner and from the same spectra as were used in the present study.

We discussed the possible sources of uncertainties and errors in our methodology in detail, and also we compared our results with those presented in other works to ensure consistency and reliability in our analysis. The large size of our sample allowed us to characterize and remove systematic abundance trends for some elements with $T_{\rm eff}$.

To separate Galactic stellar populations, we applied both purely kinematical approach and chemical method. We showed that both kinematically selected thin- and thick disks are "contaminated". The main reason of this "contamination" could be the fact that the stars in the local neighborhood have different birth radii and reached the Solar Neighborhood due to their eccentric orbits or via radial migration (e.g. Schonrich & Binney 2009).

Inspection of [X/Fe] against [Fe/H] plots suggests us that chemically separated thin- and thick disks, in addition to the Mg, Si, and Ti, are also different for Al, Sc, Co, and Ca. Some bifurcation might also exist for Na, V, Ni, and Mn, but there is no clear boundary of their [X/Fe] ratios. We observed no abundance difference between the thin- and thick disks for chromium. We found that the metal-poor α-enhanced stars and their metal-rich counterparts show different [X/Fe] trends with metallicity for different elements.

We confirmed that an overabundance in giant-planet host stars is clear for all studied elements, which lends strong support to the core-accretion model of planet formation (e.g. Pollack et al. 1996). We also confirmed that stars hosting only Neptunian-like planets may be easier to detect around stars with similar metallicity than non-planet hosts, although for some elements (particularly α-elements) we observed an abrupt lower limit of [X/H], which may indicate that these elements are important in their formation. The maximum abundance difference between Neptunian-like planet hosts and non-host stars is observed for Mg ([Mg/H] $\approx$ 0.09 dex).

Acknowledgements. This work was supported by the European Research Council/European Community under the FP7 through Starting Grant agreement number 239953. N.C.S. also acknowledges the support from Fundação para a Ciência e a Tecnologia (FCT) through program Ciência 2007 funded by FCT/MCTES (Portugal) and POPH/FSE (EC), and in the form of grant reference PTDC/CTE-AST/098528/2008. V.Zh.A., S.G.S. and E.D.M are supported by grants SFRH/BPD/70574/2010, SFRH/BPD/47611/2008 and SFRH/BPD/76606/2011 from FCT (Portugal), respectively. J.I.G.H., and G.I. acknowledge financial support from the Spanish Ministry project MICINN AYA2011-29060 and J.I.G.H. also from the Spanish Ministry of Science and Innovation (MICINN) under the 2009 Juan de la Cierva Programme. G.Kh. would like to acknowledge the support from the CAUP-11/2011-BI fellowship. We thank the anonymous referee for its useful comments and Astrid Peter for the help concerning English.

References

Adibekyan, V. Zh., Santos, N. C., Sousa, S. G., & Israelian, G. 2011, A&A, 535, L11
Adibekyan, V. Zh., Santos, N. C., Sousa, S. G., et al. 2012, A&A, 543, A89
Ammons, S. M., Robinson, S. E., Strader, J., et al. 2006, ApJ, 638, 1004
Anders, E., & Grevesse, N. 1989, Geochim. Cosmochim. Acta, 53, 197
Bensby, T., Feltzing, S., & Lundström, I. 2003, A&A, 410, 527
Bensby, T., Feltzing, S., Lundström, I., & Ilyin, I. 2005, A&A, 433, 185
Bodaghee, A., Santos, N. C., Israelian, G., & Mayor, M. 2003, A&A, 404, 715
Bond, J. C., Tinney, C. G., Butler, R. P., et al. 2006, MNRAS, 370, 163
Bond, J. C., Lauretta, D. S., Tinney, C. G., et al. 2008, ApJ, 682, 1234
Boss, A. P. 1997, Science, 276, 1836
Bovy, J., Rix, H-W., Liu, C., et al. 2012a, ApJ, 753, 148
Bovy, J., Rix, H.-W., & Hogg, D. W. 2012b, ApJ, 751, 131
Buchhave, L., Latham, D. W., Johansen, A., et al. 2012, Nature, 486, 375
Buser, R., Rong, J., & Karaali, S. 1999, A&A, 348, 98
Cayrel, R., Depagne, E., Spite, M., et al. 2004, A&A, 416, 1117
Delgado Mena, E., Israelian, G., González Hernández, J. I., et al. 2010, ApJ, 725, 2349
Ecuvillon, A., Israelian, G., Pont, F., Santos, N. C., & Mayor, M. 2007, A&A, 461, 171
Feltzing, S., Bensby, T., & Lundström, I. 2003, A&A, 397, 1
Fischer, D. A., & Valenti, J. 2005, ApJ, 622, 1102
Fuhrmann, K. 1998, A&A, 338, 161
Gazzano, J. 2011, Ph.D. Thesis, Marseille
Gazzano, J., de Laverny, P., Deleuil, M., et al. 2010, A&A, 523, A91
Ghezzi, L., Cunha, K., Smith, V. V., et al. 2010, ApJ, 720, 1290
Gilli, G., Israelian, G., Ecuvillon, A., Santos, N. C., & Mayor, M. 2006, A&A, 449, 723
Gonzalez, G. 1998, A&A, 334, 221
Gonzalez, G. 2009, MNRAS, 399, L103
Gonzalez, G., Laws, C., Tyagi, S., & Reddy, B. E. 2001, AJ, 121, 432
González Hernández, J. I., Israelian, G., Santos, N. C., et al. 2010, ApJ, 720, 1592
Haywood, M. 2008a, A&A, 482, 673
Haywood, M. 2008b, MNRAS, 388, 1175
Hog, E., Kuzmin, A., Bastian, U., et al. 1998, A&A, 335, 65
Ida, S., & Lin, D. N. C. 2004, ApJ, 616, 567
Johnson, J. A. 2002, ApJS, 139, 219
Johnson, J. A., Aller, K. M., Howard, A. W., & Crepp, J. R. 2010, PASJ, 122, 905
Jurić, M., Ivezić, Ž., Brooks, A., et al. 2008, ApJ, 673, 864
Kang, W., Lee, S. G., & Kim, K. M. 2011, ApJ, 736, 87
Kurucz, R. 1993, ATLAS9 Stellar Atmosphere Programs and 2 km s^{-1} grid, Kurucz CD-ROM No. 13, Cambridge, Mass.: Smithsonian Astrophysical Observatory, 13
Lai, K. D., Bolte, M., Johnson, J. A., et al. 2008, ApJ, 681, 1524
Laws, C., Gonzalez, G.,Walker, K. M., et al. 2003, AJ, 125, 2664
Lee, Y. S., Beers, T. C., An, D., et al. 2011, ApJ, 738, 187
Liu, C., & van de Ven, G. 2012, MNRAS, submitted [arXiv:1201.1635]
Lo Curto, G., Mayor, M., Benz, W., et al. 2010, A&A, 512, A48
Lovis, C., Mayor, M., Pepe, F., et al. 2006, Nature, 441, 305
Mayor, M., & Queloz, D. 1995, Nature, 378, 355
Mayor, M., Pepe, F., Queloz, D., et al. 2003, The Messenger, 114, 20
Mayor, M., Bonfils, X., Forveille, T., et al. 2009, A&A, 507, 487
Mayor, M., Marmier, M., Lovis, C., et al. 2011, A&A, submitted [arXiv:1109.2497]
Mishenina, T. V., Soubiran, C., Kovtyukh, V. V., & Korotin, S. A. 2004, A&A, 418, 551
Mordasini, C., Alibert, Y., & Benz, W. 2009, A&A, 501, 1139
Navarro, J. F., Abadi, M. G., Venn, K. A., et al. 2011, MNRAS, 412, 1203
Neves, V., Santos, N. C., Sousa, S. G., Correia, A. C. M., & Israelian, G. 2009, A&A, 497, 563
Ojha, D. K., Bienaymé, O., Robin, A. C., Creze, M., & Mohan, V. 1996, A&A, 311, 456
Petigura, E. A., & Marcy, G. W. 2011, ApJ, 735, 41
Pollack, J. B., Hubickyj, O., Bodenheimer, P., et al. 1996, Icarus, 124, 62
Preston, G. W., Sneden, C., Thompson, I. B., Shectman, S. A., & Burley, G. S. 2006, AJ, 132, 85
Prochaska, J. X., Naumov, S. O., Carney, B. W., McWilliam, A., & Wolfe, A. M. 2000, AJ, 120, 2513
Reddy, B. E., Lambert, D. L., & Allende Prieto, C. 2006, MNRAS, 367, 1329
Robin, A. C., Haywood, M., Crézé, M., Ojha, D. K., & Bienaymé, O. 1996, A&A, 305, 125
Robin, A. C., Reylé, C., Derrière, S., & Picaud, S. 2003, A&A, 409, 523
Santos, N. C., Israelian, G., & Mayor, M. 2001, A&A, 373, 1019
Santos, N. C., Israelian, G., Mayor, M., Rebolo, R., & Udry, S. 2003, A&A, 398, 363
Santos, N. C., Israelian, G., & Mayor, M. 2004a, A&A, 415, 1153
Santos, N. C., Bouchy, F., Mayor, M., et al. 2004b, A&A, 426, L19
Santos, N. C., Israelian, G., Mayor, M., et al. 2005, A&A, 437, 1127
Santos, N. C., Mayor, M., Bonfils, X., et al. 2011, A&A, 526, A112
Schwarzschild, K. 1907, Göttingen Nachr., 614
Schönrich, R., & Binney, J. 2009, MNRAS, 396, 203
Schönrich, R., Binney, J., & Dehnen, W. 2010, MNRAS, 403, 1829
Sneden, C. 1973, Ph.D. Thesis, Univ. of Texas
Soubiran, C., Bienaymé, O., & Siebert, A. 2003, A&A, 398, 141
Sousa, S. G., Santos, N. C., Israelian, G., et al. 2007, A&A, 469, 783
Sousa, S. G., Santos, N. C., Mayor, M., et al. 2008, A&A, 487, 373
Sousa, S. G., Santos, N. C., Israelian, G., et al. 2011a, A&A, 533, A141
Sousa, S. G., Santos, N. C., Israelian, G., et al. 2011b, A&A, 526, A99
Suda, T., Yamada, S., Katsuta, Y., et al. 2011, MNRAS, 412, 843
Takeda, Y. 2007, PASJ, 59, 335
Udry, S., Mayor, M., Queloz, D., Naef, D., & Santos, N. 2000, Conf. Proc.: The VLT opening symposium, 571
Udry, S., Mayor, M., Benz, W., et al. 2006, A&A, 447, 361
Valenti, J. A., & Fischer, D. A. 2005, VizieR Online Data Catalog, 215, 90141
van Leeuwen, F. 2007, A&A, 474, 653

Pages 15 to 15 are available in the electronic edition of the journal at http://www.aanda.org

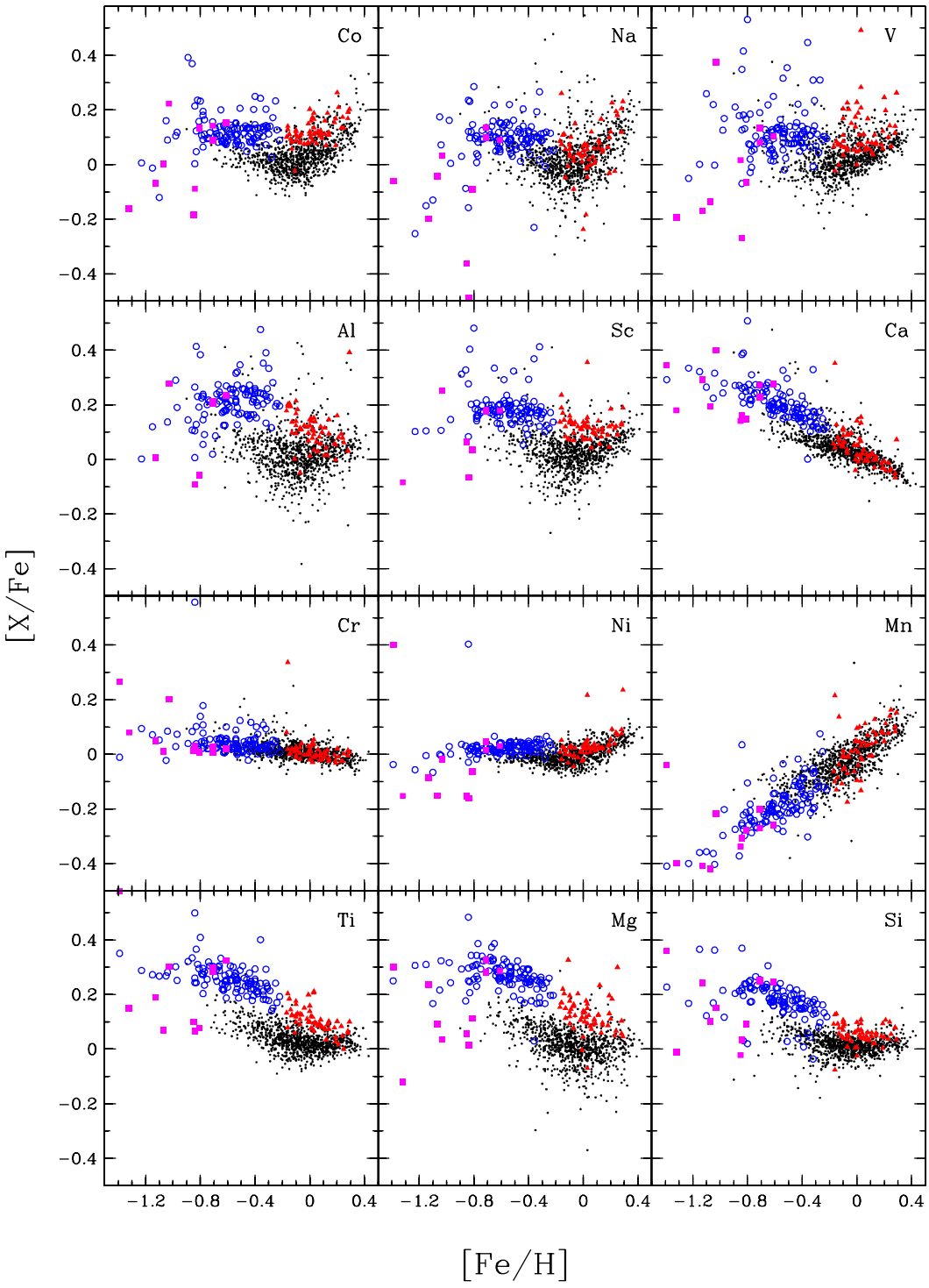

Fig. A.1. Same as Fig. 8 but for the whole sample.